Highly Tunable Fiber-Coupled Photomixers with Coherent Terahertz Output Power

S. Verghese, *Member, IEEE,* K. A. McIntosh, and E. R. Brown, *Member, IEEE*

***Abstract*—Low-temperature-grown (LTG) GaAs is used as an optical-heterodyne converter or photomixer, to generate coherent continuous-wave (CW) output radiation at frequencies up to 5 THz. Photomixers consist of an epitaxial LTG-GaAs layer that is patterned with interdigitated metal electrodes, on which two laser beams are focused with their frequencies offset by the desired difference frequency. The difference-frequency power is coupled out of the photomixer using coplanar waveguide at low frequencies and using log-spiral, dipole, and slot antennas at higher frequencies. Difference-frequency power is limited by the maximum optical-pump power that the photomixer can withstand. Fiber-coupled photomixers were operated at 77 K—a configuration in which they exhibited improved heatsinking and, therefore, withstood higher pump power. Progress has been made in the development of photomixer local oscillators (LO's) for space-based receivers that use superconducting tunnel junctions and hot-electron bolometers as heterodyne detectors.**

***Index Terms*—Gallium materials/devices, HF transmitters, optical demodulation, photoconducting devices, photomixers, photomixing.**

I. Introduction

THE spectral region 30–1000 μm lies beyond the capabilities of both solid-state lasers on the short-wavelength side and of electronic sources such as Gunn or IMPATT diodes on the long-wavelength side. Continuous spectral coverage of this region is usually achieved with black-body sources and Fourier-transform spectrometers. Discrete frequencies are obtained with molecular gas lasers. A tunable coherent solid-state source would enable high-resolution molecular spectroscopy to be performed with much shorter acquisition time than is currently possible [1]. Also, recent advances in THz receivers [2]–[5] based on superconducting bolometers have created a compelling need for a tunable single-frequency local oscillator (LO) with output power > 1 μW from roughly 0.5–3 THz.

The photomixer is a compact solid-state source that uses two single-frequency tunable diode lasers to generate a THz difference frequency by photoconductive mixing in low-temperature-grown (LTG) GaAs [6]–[9]. Compared to other fast photoconductors, high-quality LTG GaAs is well suited to this application because of its short carrier lifetime ($<$ 0.25 ps), high electrical breakdown field ($> 5 \times 10^5$ V/cm), and its relatively high mobility (> 200 cm^2 V^{-1} s^{-1}) [9]. A planar LTG-GaAs photoconductor also couples very naturally to planar antennas, acting like a current generator with very wide instantaneous bandwidth.

Photomixer development is in a research mode and the technology is still evolving. Present photomixers, however, are within reach of an important NASA application—the development of a tunable LO for superconducting heterodyne receivers operating in the submillimeter band. Photomixer LO's are being considered for use with satellite-based receivers operating from roughly 0.4–2.7 THz. This application promises to drive photomixer development to the point where it may find use in other lower cost systems.

This paper describes progress to date in advancing the capabilities of photomixers. First, the basic operation of the photomixer is summarized with references to key results from earlier work. Next, two key issues—frequency stability and output power—are addressed, which determine the photomixer's usefulness as a submillimeter-wave LO. Thermal measurements are then described, which indicate how photomixers grown on GaAs substrates undergo a thermally induced failure at high optical pump power. Finally, a brief description is given of ongoing integration of the photomixer with submillimeter-wave receivers.

II. LTG-GaAs Photomixer

The LTG-GaAs photomixer can be implemented in a variety of ways, depending on the design of its three basic parts, which include: 1) an optical system for combining and delivering two continuous-wave (CW) laser beams with optical frequencies ν_1 and ν_2; 2) an electrode design that efficiently converts the photoconductive-beat signal at ν_1–ν_2 to an RF current; and 3) an RF-output coupler. Two examples of photomixer designs that have been fabricated are shown in Fig. 1. A low-frequency version that was measured between 100 MHz and 20 GHz has a 20×20 μm active area with forty 0.2-μm interdigitated metal electrodes separated by 0.3-μm gaps. The electrodes are connected to a planar distributed circuit—in this case, a coplanar waveguide with a smooth transition to a coaxial-type connector that was used to measure the output power on a spectrum analyzer. The output power has little frequency dependence over the low-frequency band. Fig. 1(b) shows a high-frequency (HF) design that operates from approximately 0.1–5 THz. Here, the active area is at the driving point of a self-complementary log-spiral antenna that presents a resistive load over much of the submillimeter band. Due to its high

Manuscript received December 4, 1996; revised May 1, 1997. This work was supported by the National Aeronautics and Space Administration, Office of Space Access and Technology, through the Center for Space Microelectronics Technology, Jet Propulsion Laboratory, California Institute of Technology.

S. Verghese and K. A. McIntosh are with Lincoln Laboratory, Massachusetts Institute of Technology, Lexington, MA 02173 USA.

E. R. Brown is with DARPA/ETO, Arlington, VA 22203 USA, on leave from Lincoln Laboratory, Massachusetts Institute of Technology, Lexington, MA 02173 USA.

Publisher Item Identifier S 0018-9480(97)06000-6.

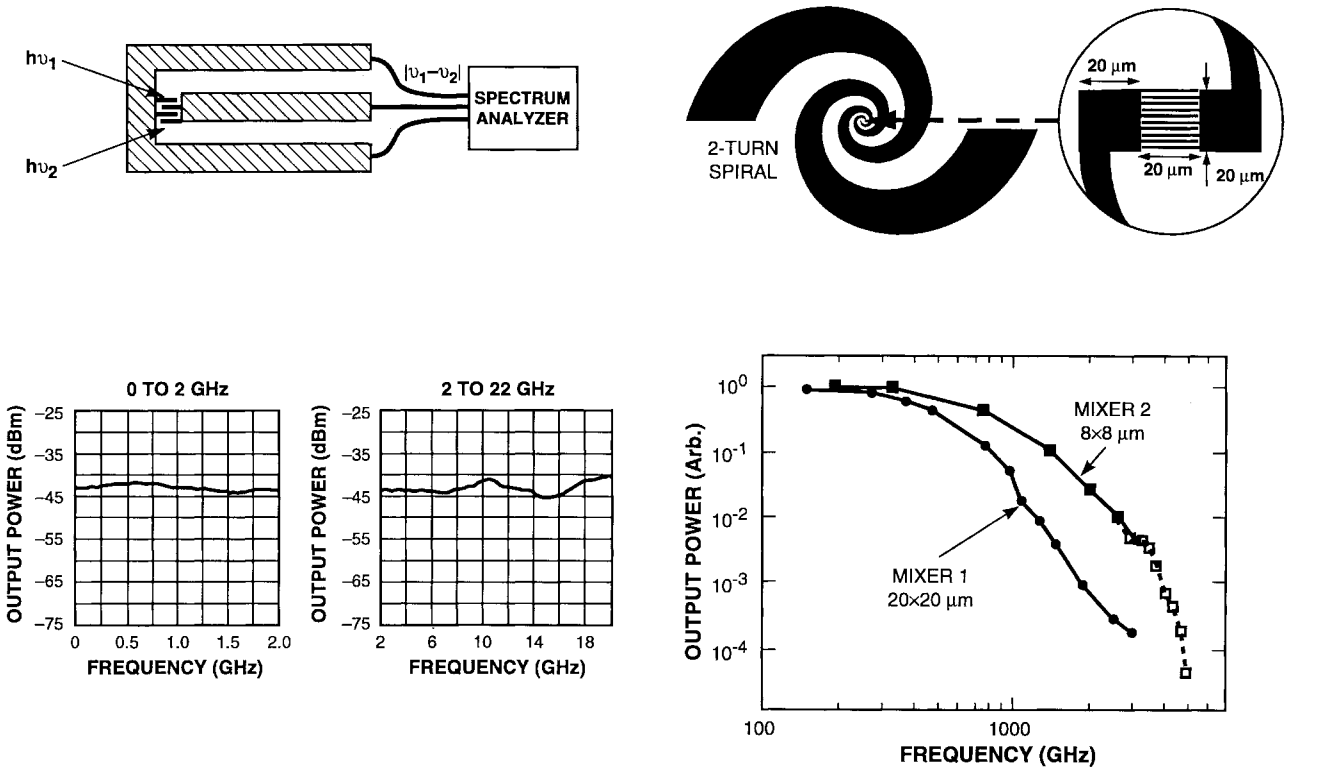

(a) (b)

Fig. 1. (a) Photomixer packaged in coplanar waveguide for low-frequency operation. The bandwidth curve was measured on a spectrum analyzer. (b) Spiral-antenna-coupled photomixer for HF operation. Pictured is mixer 1, comprising a 20 × 20 μm active area with 1.8-μm gaps between 0.2-μm-wide metallic electrodes ($C = 2.9$ fF). Mixer 2 uses the same electrode geometry, but the area is only 8 × 8 μm ($C = 0.5$ fF). The normalized bandwidth curves were measured with a 4.2-K bolometer.

dielectric constant ($\varepsilon_r = 12.8$), the GaAs substrate collects most of the radiated power, which then couples through a Si hyperhemispherical lens that partially collimates the beam. A pigtailed optical fiber couples the laser pump light to the photomixer.

A. Optical Heterodyne Conversion

The photomixing process occurs during illumination of the interdigitated-electrode region with two single-mode CW laser beams having average powers P_1 and P_2 and frequencies ν_1 and ν_2, respectively. The instantaneous optical power incident on the photomixer is given by [10]

$$P_i = P_0 + 2\sqrt{mP_1P_2}[\cos 2\pi(\nu_1 - \nu_2)\mathrm{t} + \cos 2\pi(\nu_1 + \nu_2)\mathrm{t}] \tag{1}$$

where m is the mixing efficiency that ranges in value between 0 and 1 depending on the spatial overlap of the two laser-mode fields. The first cosine term modulates the photoconductance at the difference frequency, and the second term appears at approximately twice the optical frequency and does not couple to the RF circuit. Solving the current–continuity equation yields the small-signal result of optical heterodyne theory for the photomixer [11]

$$P_\omega = \frac{1}{2}(G_0V_B)^2R_A/[1+\omega^2\tau_e^2][1+(\omega R_AC)^2]. \tag{2}$$

Here, V_B is the dc voltage bias across the electrodes, G_0 is the dc photoconductance for an average incident power P_0, R_A is the antenna–radiation resistance (72 Ω for a self-complementary antenna on GaAs), τ_e is the carrier lifetime, and C is the fringe capacitance of the interdigitated electrode structure. Equation (2) is valid for moderate optical power such that $G_0R_A \ll 1$. To date, all experimental measurements have been made in this limit. In the limit of HF, where $\omega\tau_e \gg 1$ and $\omega R_AC \gg 1$, the difference-frequency power P_ω is proportional to ω^{-4} and drops at 12 dB/octave. HF operation, therefore, requires that the photomixer has low values of τ_e and C. In the limit of low frequencies, the available difference-frequency power can be conveniently estimated by measurement of the dc photocurrent $I_{\mathrm{dc}} = V_BG_0$. Then the output power is simply $P_\omega = 0.5\, I_{\mathrm{dc}}^2R_A$.

A careful comparison of theory and measurement was made for a low-frequency photomixer of the type shown in Fig. 1(a), but with a 20 μm × 20 μm electrode geometry consisting of ten 1.0-μm-wide electrodes and nine 1.0-μm-wide gaps [11]. Optical illumination was supplied by two adjacent cavity modes of a CW Ti:sapphire laser that had a frequency spacing of 200 MHz centered at approximately $\lambda = 780$ nm. For a bias voltage of 36 V (3.6×10^5 V · cm^{-1}), there was close agreement with theory up to a total optical power of approximately 50 mW. For higher power, the theory slightly overestimated P_ω up to the maximum sustainable power for this particular device ($P_0 \approx 170$ mW). The disagreement has been observed in many of our devices for electric-field

strengths approximately above 3×10^5 V $\cdot$ cm^{-1}. The device failed at $P_0 > 170$ mW. The temperature during device failure was estimated to be 87 K above room temperature using a thermal model for spreading resistance and assuming a thermal conductivity for GaAs of 0.46 W $\cdot$ cm^{-1} K^{-1} at 300 K.

B. Electrode Geometry and Photocarrier Lifetime

For terahertz (THz) photomixer applications, the most important characteristic of the material is the photoelectron lifetime τ_e. For each photomixer wafer, this quantity is measured using time-resolved photoreflectance before the submicron lithography steps are performed. Wafers sent to fabrication routinely have measured lifetimes $\tau_e = 200$–300 fs, although lifetimes as short as 90 fs have been measured on our best wafers [11]. For THz operation, the most important characteristic of the electrode geometry is the capacitance. Many different electrode geometries have been fabricated—with active areas between 4 $\times$ 4 and 20 $\times$ 20 μm, gaps between 0.3 and 8 μm μm, and finger widths between 0.2–1 μm [6], [7], [9]. The best performance from a spiral-coupled device above 1 THz has been achieved with an 8 $\times$ 8 μm area, 1.8-μm gap, and 0.2-μm finger width. This design represents a compromise between a large value of G_0 and a small value of C. For low-frequency operation, a larger area device with many fingers would give both a large current responsivity and a high damage threshold for optical pump power. The 8 μm $\times$ 8 μm device, however, outperforms the 20 μm $\times$ 20 μm device above 1 THz because of its smaller capacitance [6]. The plot in Fig. 1(b) compares the normalized output power of a 20 μm $\times$ 20 μm device (mixer 1) with an 8 $\times$ 8 μm device (mixer 2) and clearly shows the effect of electrode capacitance.

C. Quadratic Bias Dependence

An interesting nonohmic behavior is routinely observed in the dc I–V characteristic of some photomixers at high bias voltage. For example, a quadratic dependence of the dc photocurrent on bias voltage was observed above 5 V in a device with a gap width of 0.6 μm and above 2 V in a 0.3-μm-gap device [9]. At a difference frequency of 200 MHz, the quadratic dc I–V curve translated into a quartic dependence of the output power on bias voltage as would be expected from (2) if $G_0 V_B$ were replaced with $(G_0 V_B + G_1 V_B^2)$, where G_1 represents the nonlinear conductance. An explanation based in part on the Mott–Gurney theory attributes nonohmic transport to the buildup of space charge between the electron-injecting contacts [13]. A theoretical description of this effect in photomixers has been published elsewhere [9], but a brief physical description is given here. The effect is due, in part, to the different lifetimes for mobile electrons and holes [14] that can result from the indirect recombination process that involves deep traps in LTG GaAs. Ohmic behavior is observed for small bias voltages where the transit time between electrodes is longer than the lifetime for both electrons (τ_e) and holes (τ_h), and the collection region between the electrodes is essentially space–charge neutral. A region of negative space charge begins to form at higher voltage when the holes are swept out of the collection region before they can recombine with the trapped electrons—that is, $\tau_{th} < \tau_h - \tau_e$, where τ_{th} is the transit time for holes. Above this voltage, the collection region is no longer space–charge neutral and a quadratic bias dependence on voltage occurs for the photocurrent. The resulting quartic dependence on voltage of the photomixer-output power is essential in explaining the milliwatt-level power that has been observed at 200 MHz [9] and also the bias dependence of the output power observed at millimeter wavelengths. The quartic bias dependence, however, is not expected to persist at THz frequencies. The reason is that in the nonohmic regime, the photomixer no longer behaves as a simple photoconductor—instead, it develops some of the characteristics of transit-time devices. Therefore, a quartic bias dependence in the output power should only occur if the difference frequency satisfies the condition $\nu_1 - \nu_2 \ll \tau_{th}^{-1}$. Indeed, measurements performed on our photomixers with high bias voltage show a bias dependence that is weaker than quartic at THz frequencies. A detailed investigation of this effect is in progress. There are other mechanisms for nonohmic dc characteristics in LTG GaAs that have been reported by Ibbetson and Mishra [15]. It is not yet clear how these mechanisms affect the photomixer output.

III. Key Issues for Photomixer Local Oscillators

An important application for photomixers is that of a tunable LO system for submillimeter-wave receivers on satellite platforms. These instruments are being considered by NASA for use in astrophysics, atmospheric chemistry, and terrestrial radiometry. At present, the most successful LO technology in the range of 0.2–0.8 THz is harmonic multiplication using Schottky-diode varactors and Gunn-diode master oscillators that operate near 100 GHz [16]. Such LO's can be phase locked to a reference frequency and provide adequate LO power for superconducting receivers operating up to approximately 0.8 THz. At higher frequencies (0.8–1.2 THz), both the output power and the tuning range suffer. Resonant-tunneling diodes have operated up to 712 GHz, but parasitics make much higher frequency operation unlikely [17]. Gas lasers operating on molecular lines are used at still higher frequencies (e.g., 2.5 THz). These sources provide ample output power but are limited to fixed frequencies, have considerable mass, and consume hundreds of watts of wall-socket power.

Compared to these technologies, the photomixer has the all-solid-state advantages of the multiplier systems, the HF capability of the gas lasers, and a wide tuning range that is unique to itself. In the past five years, rapid progress in photomixer development has demonstrated, in principle, the feasibility of compact LO's that operate between 0.1 and 3 THz. Some key issues, however, must still be resolved before the photomixer will find its way into engineering models of the above-mentioned instruments. The two most pressing issues are the frequency stability of the diode lasers, and the available output power from the photomixer at frequencies above 1 THz.

A. Amplitude and Frequency Stability

Most of the photomixer measurements have been made at $\lambda \approx$ 780–820 nm using two continuous wave (CW)

Ti:sapphire lasers—a standing-wave laser and a tunable ring laser pumped by a single Ar laser. In the last two years, commercially available diode lasers that operate at $\lambda \approx$ 850 nm have been used [6]. No difference was observed in the swept power spectrum of the photomixer between illumination from the Ti:sapphire lasers and from the diode lasers. The diode lasers are of the distributed Bragg reflector (DBR) type and are available with CW power up to 150 mW [18].[1] A pair of them can be temperature and current tuned over a range of approximately 1.5 THz of difference frequency. A 3-THz tuning bandwidth was achieved by using three such lasers with appropriately selected center wavelengths. The amplitude stability of the diode-laser output is superior to that of the Ti-sapphire lasers. This is beneficial since the laser-amplitude stability determines the stability of the photomixer output. The amplitude noise arises from rms current noise in the laser-bias circuitry. Low-noise current sources are used, which contribute only about 2×10^{-5} rms relative-intensity noise in a 200-kHz noise bandwidth.[2]

A concern with many diode lasers is their susceptibility to optical-feedback-induced instabilities. The DBR lasers are less sensitive to optical feedback than standard Fabry–Perot diode lasers. With free-space pumping, however, a Si_3N_4 antireflection coating on the photomixer surface was necessary to maintain single-frequency operation. The spectral purity of the DBR pump lasers was measured by coupling the output of a low-frequency photomixer [Fig. 1(a)] directly into a spectrum analyzer operating at 15 GHz. In a 20-ms sweep of the analyzer, a full width at 10-dB down of 100 kHz was observed—although the resolution was limited by the analyzer. In a 1-min integration, the peak fluctuated in a 50-MHz bandwidth, which is dictated primarily by fluctuations in the temperatures of the lasers. Similar results were obtained at 91 GHz using a fiber-coupled photomixer with a spiral antenna when the output was measured with a W-band Schottky receiver. In this case, it was necessary to use an optical isolator with approximately 38-dB reflection isolation between the DBR lasers and the input of the connectorized optical fiber. Application of a feedback loop in the laser drive circuit should allow the linewidth of the output radiation to be stabilized at the 100-kHz instantaneous linewidth or better, provided an appropriate error signal can be generated. Such a linewidth would be adequate for many radiometer measurements in, for example, atmospheric chemistry.

Several collaborating groups are independently developing frequency-locking techniques for diode lasers that operate at various difference frequencies. Waltman *et al.* [19] have demonstrated a locking technique that slaves the frequency of one diode laser to the other, separated by the desired difference frequency. The error signal is obtained by mixing the output of the photomixer with a harmonic of a Gunn oscillator on a Schottky-diode mixer. The output of the mixer is then fed back to the bias current of one of the lasers. This approach has stabilized two external-cavity diode lasers to a 10-dB linewidth of $<$ 100 kHz at a difference frequency of 364 GHz. The linewidth was limited by the phase noise of the Gunn oscillator, which can be locked to a low phase-noise synthesis chain to obtain linewidths as narrow as a few hertz. The signal-to-noise ratio of the Schottky mixer is ample at 364 GHz, but rolls off rapidly with frequency. Consequently, this technique appears promising for frequencies below 1 THz. For higher frequency operation, a technique using resonant optical feedback appears promising [20]–[22]. In this technique, each laser diode is stabilized with a high-finesse confocal resonator that is tuned with a piezoelectric transducer on a cavity optic. This system has shown short-term (20-ms) frequency stability of approximately 50 kHz and longer term (10-s) stability of approximately 2 MHz. Excellent long-term stability is expected from a three-laser technique which uses multiple orders of a high-finesse cavity that is stabilized to the hyperfine transition of Cs. This technique will also allow for accurate determination of the generated difference frequency.

B. Submillimeter-Wave Output Power

Much current research is focused on increasing the available output power of the photomixer at frequencies above 1 THz. Below 1 THz, output powers of approximately 1 μW for 8 $\times$ 8 μm photomixers grown on semi-insulating GaAs substrates and coupled to log-spiral antennas are routinely measured. The output power is limited by the maximum optical power that these devices can withstand before failure—approximately 60 mW at room temperature. At frequencies near 500 GHz and lower, the photomixer currently has enough available LO power to pump superconductor–insulator–superconductor (SIS) mixers. At higher frequency, however, the required LO power for SIS mixers increases in proportion to the square of the frequency. Superconducting hot-electron bolometers are being developed as heterodyne receivers for frequencies between roughly 700 GHz and 2.7 THz [2]–[5]. The required LO power for these devices is not yet available from the photomixer. Two approaches have been pursued, which have produced significant increases in output power and hold promise for further optimization. The first approach uses resonant antennas that have higher impedance than broadband spiral antennas, yet still have enough bandwidth to cover a waveguide band. The second approach is to improve the capability of the substrate material to function as a heatsink for the optical pumps—either by cooling or by using a composite substrate.

The output power from the photomixer was measured with a 4.2-K composite bolometer.[3] The bolometer was mounted in an integrating cavity with a 2-mm-diameter input aperture. Incident radiation is directly imaged onto the aperture through cold baffles so that the optical throughput is 0.0011 sr-cm^2. This results in sensitivity to only one spatial mode up to frequencies of roughly 1 THz—a useful property for measuring antenna-beam patterns. Standing waves are a problem below $\sim$300 GHz because of the integrating cavity. At low frequencies, a calibration of the bolometer responsivity was made using a series of three IMPATT oscillators covering a frequency range between 91–109 GHz. The output power from

[1] SDL, Inc., San Jose, CA 95134-1365.

[2] Model LDC 3900 modular laser diode controller, ILX Lightwave, Bozeman, MT 59771.

[3] Si composite bolometer, Infrared Laboratories, Inc., Tucson, AZ 85719.

these oscillators was monitored with a waveguide-mounted W-band power meter and was coupled to the bolometer with a feedhorn and a dielectric lens that reimaged the beam waist onto the bolometer aperture. Further calibrations of the bolometer were made by using RTD oscillators that were monitored by calibrated Schottky mixers at several frequency points up to 407 GHz. For HF calibration, a far-infrared methanol-gas laser monitored by a Scientech power meter was used to provide a calibration for the bolometer at 2.5 THz. A careful attempt at calibration was made at each frequency point, but it is possible that errors of ~3-dB magnitude were introduced due to the differences in the optical coupling of the various sources and detectors. Across the 100-GHz–2.5-THz band, the optical responsivity of the bolometer was measured to be approximately 15 dB less than the electrical responsivity that was derived from its current–voltage characteristic [23].

The log spiral is a type of planar antenna whose useful range can exceed a decade of bandwidth. When fabricated on a GaAs wafer, the driving-point resistance of the spiral antenna is approximately $R_A = 60\pi/(\varepsilon_{\text{eff}})^{1/2} \approx 72\ \Omega$, where ε_{eff} is the effective dielectric constant given by $(1+\varepsilon)/2$. A typical illuminated 8 μm × 8 μm device with 1.8-μm gaps has a dc photoconductance of $G_0 \approx (40\ k\Omega)^{-1}$. In the limit $G_0 R_A \ll 1$, the output power radiated by the photomixer should depend linearly on the antenna driving-point resistance: $P_\omega \propto I_{\text{dc}}^2 R_A/2$. Resonant slot and dipole antennas offer higher values of R_A and have been measured extensively in the microwave and millimeter-wave region [24] and, to some extent, at THz frequencies [25], [26].

Planar slot antennas were designed that would operate near their half-wave resonance, and dipoles were designed to operate near their full-wave resonance [27]. These antennas were expected to yield larger values for R_A over a narrower bandwidth than the spiral. Fig. 2(a) shows a comparison of the output power measured from a spiral with that measured from a 70-μm-long by 4-μm-wide slot antenna using the bolometer. The data are plotted as the ratio of the swept power spectrum for the slot antenna to the swept power spectrum for the spiral. The dc photocurrent and bias conditions were identical for both devices. The broad region of enhanced output from the slot antenna around 1 THz is the frequency band over which the slot antenna has a radiation resistance higher than the 72-Ω resistance of the spiral. A peak radiation resistance of approximately 200 Ω was measured at 1.2 THz, representing almost a threefold increase in output power. The width of the enhanced region is relatively broad—almost 2 THz. Additional slot antennas with lengths of 38 and 22 μm were fabricated and showed similar behavior with peak radiation resistances at 2.3 and 4 THz, respectively.

Several types of resonant dipoles were also investigated. Results are summarized in Fig. 2(b) from dipole antennas with bias lines that fed out from the center. Dipoles with end biasing, such as those commonly used in pulsed terahertz radiators, were also investigated. The highest peak radiation resistances, however, were measured for the center-biased dipoles. Curves are shown for dipoles with lengths of 30, 45, 90, and 180 μm. Resonant frequencies varied from 375 GHz for the longest dipole to approximately 2.5 THz for

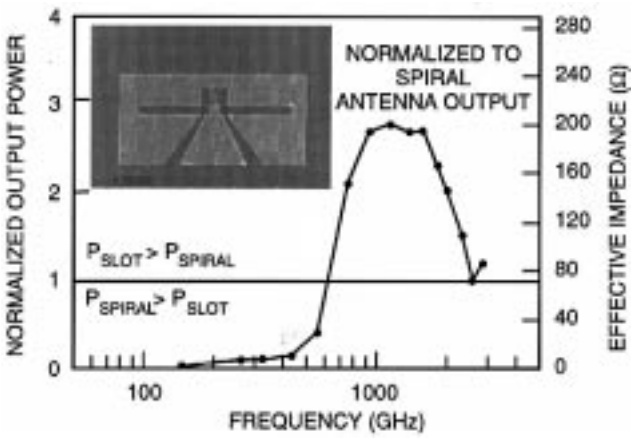

(a)

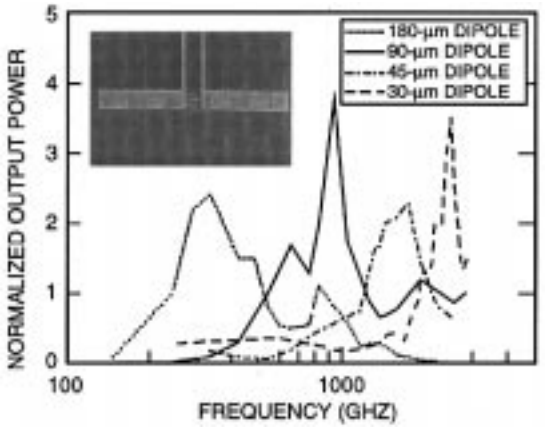

(b)

Fig. 2. (a) Output power from a slot-antenna-coupled photomixer ratioed to the output power from a spiral-coupled photomixer. The region with effective impedance above 72 Ω is where the power from the slot exceeded the power from the spiral. (b) Measured output power ratioed to a spiral for photomixers with dipoles of various lengths.

the shortest. The peak radiation resistances were ~300 Ω for dipoles operating at 0.9 and 2.5 THz. Dipoles were also fabricated with choke filters designed to prevent RF leakage through the bias lines. There was little difference, however, between the output powers measured for dipoles with and without chokes.

A second way to increase the THz output is to increase the total optical power P_0 that the photomixer can sustain before failure. The potential increase in output power is large since the available output power is proportional to P_0^2. The 8 × 8 μm photomixers with 1.8-μm gaps can withstand a total optical power of $P_0 \approx 60$ mW (9×10^4 W · cm^{-2}) at room temperature when biased at approximately 30 V. Above that power, a combination of optical and ohmic heating causes catastrophic failure of the device. Under a microscope, many failed samples show a fracture beneath the surface of the active area that left a crater, typically of diameter > 100 μm and at the center of where the active area was. The missing material broke away cleanly and was still attached to the optical fiber in the samples where fiber-optic coupling was used. Before failure, at a 30-V bias, the measured output power of the photomixer continued to increase as P_0^2, even near

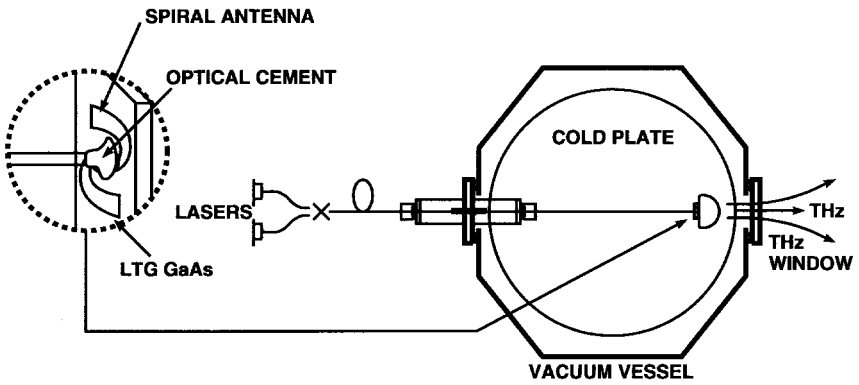

Fig. 3. Schematic diagram showing the optical coupling scheme for a fiber-coupled photomixer operating at 77 K.

the maximum P_0. This suggests that substrates with higher thermal conductivity could result in a significant increase in photomixer output power.

The thermal conductivity of GaAs is six times higher at 77 K than at 300 K [28]. Therefore, operation of photomixers at 77 K was expected to increase the maximum P_0 due to this increase and because the base temperature is reduced by 223 K. Cooled photomixers were operated in a liquid-nitrogen cryostat with an optical fiber used to couple the optical beams. Fig. 3 shows the fiber-optic coupling scheme. Combined light from two CW Ti:sapphire lasers operating between 813 and 819 nm was coupled into a 4-m length of polarization-maintaining single-mode optical fiber.[4] The fiber entered the liquid nitrogen cryostat through a hermetic feedthrough made from a 1-cm length of stainless steel tubing (diameter 1.5 mm) that was filled with low vapor-pressure epoxy. The cleaved end of the fiber was positioned over the photomixer active area and was then cemented to a position roughly 50 μm away from the surface of the chip. At this distance, the laser beam expands to approximately fill the 8 μm $\times$ 8 μm active area. The result is a robust package that allows independent alignment of the THz and optical beams and is immune to thermal motion in the cryostat. For comparison, measurements were also performed using free-space coupling of the lasers through an optical window to the photomixer. The terahertz-output power for free-space coupling is typically 1 to 3 dB higher than for fiber coupling because of the difficulty of cementing the core of the fiber precisely over the active area. This positioning problem is being addressed with an electrostrictive postioning stage, which is part of a feedback loop that maximizes the photocurrent while the cement is cured.[5]

Fig. 4 shows a comparison of the terahertz-output power for 8 μm $\times$ 8 μm photomixers with spiral antennas operating at 290 and 77 K. Curve (a) shows a swept power spectrum for a fiber-coupled photomixer operating at 290 K with a 30-V bias and an optical power of 20 mW. Curve (b) was measured for a free-space-coupled photomixer operating at 300 K with $V = 20$ V and $P_0 = 30$ mW. The bandwidth is in agreement with the fiber-coupled device. The frequency rolloff above

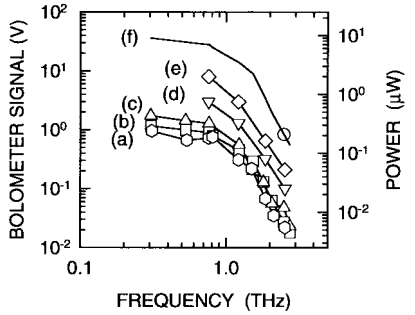

Fig. 4. Output power for room temperature and 77-K photomixers. (a) 77-K operation of a fiber-coupled photomixer with 30-V bias and $P_0 = 20$ mW. (b) 290-K operation of a free-space-coupled photomixer with 20-V bias and $P_0 = 30$ mW. (c) 77-K free-space-coupled photomixer under the same conditions as curve (b). (d) 77-K fiber-coupled photomixer, 30-V bias, and $P_0 = 40$ mW. (e) 77-K fiber-coupled photomixer, 30-V bias, 60 mW. (f) 77-K free-space coupling with 30-V bias and $P_0 \approx 90$ mW. The line shows the expected scaling to lower frequencies.

$\sim$1.5 THz is approximately 12 dB per octave, consistent with previous measurements [6]. The output power for these devices is proportional to P_0^2 and to $\sim V^2$. Therefore, curves (a) and (b) were expected to approximately agree in amplitude as well. Curve (c) is the swept-power spectrum for a free-space-coupled photomixer operating at 77 K with $V = 20$ V and $P_0 = 30$ mW. The shapes of curves (b) and (c) are similar, and the 3-dB bandwidth of $\sim$0.9 THz was preserved as the device was cooled to 77 K. This suggests that the ultrafast trapping of carriers by the defect states near the middle of the band gap is not very temperature sensitive. Indeed, time-domain photoreflectance experiments also indicate that the photoexcited-carrier lifetime has a negligible temperature dependence [29]. Curves (d) and (e) were measured for a fiber-coupled device at 77 K with pump powers of 40 and 60 mW, respectively. The amplitude of the measured output power scales as the square of the optical pump power. The 0.2-μW point on curve (f) is the highest measured power at 2.5 THz.[6] It was obtained from a free-space-coupled photomixer cooled to 77 K with $P_0 \approx 90$ mW. The curve shows the expected frequency scaling of the THz output power at lower frequencies. Measurements of the maximum optical power

[4] Single-mode polarization-maintaining optical fiber from 3M Corporation, part number FS-PM-4625.

[5] Orion fiber positioning system, Newport Corporation, Irvine, CA 92714.

[6] The 0.2-μW point has been corrected for the losses measured at 2.5 THz in the TPX vacuum window and in the vacuum grease used to mount the photomixer chip to the silicon hyperhemisphere lens.

on numerous 77-K photomixers indicate that the 8×8 μm devices can operate with between 90 and 100 mW before failure. Note that upon cooling, the realized increase in the maximum P_0 was significantly lower than expected from published values of GaAs thermal conductivity and from the reduction in the base temperature. This discrepancy points out the need to monitor the temperature of the photomixer active area during illumination by the optical pumps.

IV. Thermal-Failure Limit of the Photomixer

To investigate the thermal-failure mechanism, a two-color pump-probe measurement was used, in which the temperature of the active area could be deduced *in situ* by detecting temperature-dependent changes in the photocurrent caused by changes in the bandgap of the LTG GaAs. One color of light—the CW pump laser (Ti:sapphire, $\lambda = 810$ nm)—functioned as a heater that coupled a known amount of optical power into the active area. Deducing the absorbed power is aided by the relatively small change in the absorption coefficient of GaAs with temperature at $\lambda = 810$ nm [28].[7] A second color—the CW probe laser (DBR diode, $\lambda = 852$ nm)—functioned as a thermometer. The 852-nm photons have energy that is just above the band gap at 300 K, and slightly below the band gap at 77 K. Therefore, a large change in the current responsivity at 852 nm is expected as the photomixer is heated by the 810-nm pump laser. This technique has an important advantage over other methods of measuring thermal interface resistance or spreading resistance. In this technique, the thermal resistance is deduced by measuring the active area of the photomixer directly, with its metal electrodes, RF antenna, and fiber-pigtail joint. These all contribute to the thermal circuit of the photomixer and would be difficult to account for with a less direct measurement.

In the pump-probe measurement, a glass slide was used as a diplexer to combine a small amount (3–5 mW) of 852-nm light from the diode laser with the Ti:sapphire beam. The two-color beam was then focused into a polarization-maintaining single-mode optical fiber with the 810- and 852-nm light in orthogonal polarization states. The optical fiber went through a hermetic feedthrough into a variable-temperature cryostat cooled by a closed-cycle ^{4}He refrigerator. The fiber was cemented to the photomixer active area using the method described above. The output of the diode laser was mechanically chopped at 2.4 kHz, thereby generating an ac photocurrent that was detected with a transimpedance preamplifier and a lock-in amplifier. For a given base temperature, changes in the output of the lock-in amplifier were then monitored as a function of the incident pump power from the Ti:sapphire laser. These data were then calibrated as temperature changes by comparing them with a previous measurement of the temperature dependence of the 852-nm photocurrent. The calibration curve [Fig. 5(a)] was measured with the photomixer on a variable-temperature stage, which was heated with a resistor and cooled by the refrigerator. The diode laser power was

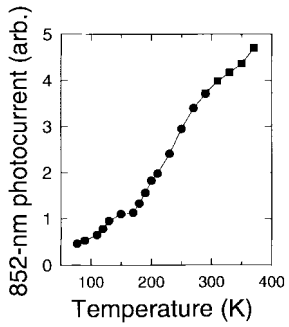

(a)

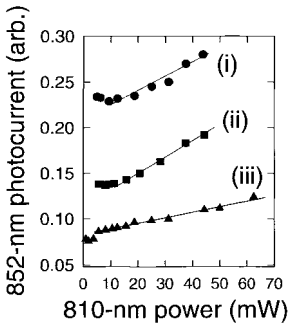

(b)

Fig. 5. Two-color measurement technique for determining the photomixer active-area temperature. (a) 852-nm photocurrent calibration curve measured with 4.5 mW chopped at 2.4 kHz. (b) 852-nm photocurrent as a function of Ti:sapphire pump power. The lines are guides to the eye and show the region where the data give information about heating. (i) 290-K base temperature. (ii) 200-K base temperature. (iii) 77-K base temperature.

4.5 mW and the photomixer temperature was scanned from 77–372 K over a period of 4 h. Various segments of the data were reproduced to check for slow drifts or hysteresis. The 852-nm photocurrent changed by approximately one order of magnitude over this range and is, therefore, a good thermometer. Fig. 5(b) shows the measured 852-nm photocurrent at various base temperatures as a function of the 810-nm pump power. The linear portions of the curves above $\sim$5 mW are used to extract a thermal conductance for heat dissipation from the photomixer active area. At very low power, there are long-lived states in the LTG GaAs that are not bleached out and make those data unusable. Curve (i) shows data for the fiber-coupled photomixer measured at 290 K. As the pump power was raised to 44 mW, the 852-nm photocurrent increased by 22% from its base value. Using Fig. 5(a) as a calibration, one finds that a 22% increase in photocurrent response at 290 K corresponds to a temperature rise of 82 K. Then the lumped thermal conductance for heat dissipation from the photomixer active area is $G = 5.4 \times 10^{-4}$ W/K. A value of $G = 5.0 \times 10^{-4}$ W/K was measured under identical conditions for a different chip from the same molecular-beam epitaxy (MBE) growth run. The expected value from a simple spreading-resistance calculation is $G = 6.9 \times 10^{-4}$ W/K, given an uniform laser spot with diameter of 6 μm on the active area.[8]

[7] For a 1.5-μm-thick GaAs film, the calculated reduction in absorbed power from 300 to 77 K is approximately 11%.

[8] The spreading resistance can be modeled by assuming the active area is a hot hemisphere of area A that emits heat by conduction into a semi-infinite substrate with thermal conductivity k. Then, the thermal conductance at zero frequency is $G = k(2\pi A)^{1/2}$. At 290 K, $k = 0.46$ W cm^{-1} K^{-1} for GaAs.

TABLE I
RESULTS OF TWO-COLOR PUMP-PROBE MEASUREMENTS FOR VARIOUS BASE TEMPERATURES AND PUMP POWERS. THE BOLD ENTRIES ARE FOR OPERATION WITH PUMP POWER NEAR THE THERMAL-FAILURE POINT

Substrate	Base Temp	Pump Power	Temp Rise	G (W/K)
GaAs	290 K	44 mW	82 K	$5.4\text{x}10^{-4}$
GaAs	200 K	44 mW	40 K	$11\text{x}10^{-4}$
GaAs	77 K	44 mW	12 K	$37\text{x}10^{-4}$
GaAs	77 K	63 mW	33 K	$19\text{x}10^{-4}$
GaAs	**290 K**	**60 mW**	(112 K)	($5.4\text{x}10^{-4}$)
GaAs	**77 K**	**90 mW**	**108 K**	$\mathbf{8.3\text{x}10^{-4}}$

Table I summarizes results from the two-color measurements for several different base temperatures and pump powers. For the moderate pump power of 44 mW, the deduced values of G scale with temperature in rough agreement with bulk thermal conductivity values in the literature [28]. Thermal modeling of this system as a standard spreading resistance problem shows that most of the temperature drop occurs within roughly $\sim 10\ \mu$m from the surface. This creates a large temperature gradient right below the active area of the photomixer. Note that the 77-K data with 63 mW of pump power give a smaller value of G than that measured at 77 K with 44 mW. This is a consequence of the strong temperature dependence of the thermal conductivity of GaAs. A complete solution of the resulting nonlinear differential equation would, in principle, show this effect. The entries shown in bold are for operation near the thermal-failure point. For 290-K operation, the entry for the temperature rise is an estimate ($\Delta T = 112$ K). It was calculated using the value $G = 5.4 \times 10^{-4}$ W/K measured at 44 mW. The last row in the table is for a two-color measurement that was performed on the device at 77 K just before thermal failure. The measured temperature rise was 108 K—corresponding to an active-area temperature of only 185 K. This is a strong indicator that the thermal-failure mechanism is not dependent on the absolute temperature of the active area. Instead, the material seems to fracture and fail when a temperature difference of roughly 110 K causes a severe thermal gradient to occur within 10 μm of the surface. The thermal fracture may be a result of residual strain in the epitaxial layers after MBE growth.

Recently, LTG-GaAs samples were grown in the MBE system on silicon substrates [30]. Photomixer electrodes were fabricated on these samples and optical fibers were attached. These samples withstood 110–120 mW of optical pump power at 290 K before failing. The difference-frequency output was monitored at 200 MHz for one of the samples and it showed the expected increase as a function of pump power. This device could not be used for HF measurements because the Si substrate was absorbing at terahertz frequencies due to its high doping. At present, it is not clear if the increase in maximum optical power is a result of the superior thermal conductivity of Si compared to GaAs, or if the structural toughness of the Si samples makes thermally induced fracture less likely. Two-color pump-probe measurements are in progress for the silicon-substrate photomixer.

V. FUTURE DIRECTIONS

Currently, photomixer development is focused on LO's for heterodyne receivers that will operate between 0.4–2.7 THz and be used primarily on satellites and airborne platforms. An important milestone in this application is the integration of photomixers with superconducting receivers. A preliminary integration experiment was performed in collaboration with the Harvard–Smithsonian Center of Astrophysics, Cambride, MA, using a 290-K photomixer LO and a SIS heterodyne detector operating at 513 GHz [31]. The photomixer power was coupled quasioptically through a resonant diplexer. The measured double-side-band (DSB) noise temperature was 650 K, a result limited by the amount of LO power that was coupled to the SIS detector ($\sim$ 10 nW) from that unoptimized photomixer. With $\sim$4 dB more LO power, the expected noise temperature would be approximately 200 K DSB. Integration experiments are also under way for frequencies above 1 THz with collaborators from the Jet Propulsion Laboratory, Pasadena, CA, using photomixers coupled to superconducting hot-electron bolometers. It is estimated that these mixers will require approximately 2-μW LO power from the photomixer between 1–2.7 THz [32]. The integration experiments require better frequency stability from the diode lasers and more output power from the photomixer. To this end, progress by other research groups in frequency locking the laser diodes will be incorporated into a photomixer–LO breadboard [19].

At terahertz frequencies, metallic waveguides are lossy and quasioptical systems, that use Gaussian beam, guide and combine the LO and signal in heterodyne systems [33]. For most applications, the photomixer LO should, therefore, radiate into a Gaussian mode [25]. A nearly Gaussian radiation pattern was measured from the single-dipole and spiral antennas [27]. Also, planar antennas such as twin dipoles and twin slots are being explored for the photomixer that have Gaussian-coupling efficiency near 90%. Feedhorns can have even higher Gaussian-coupling efficiency. A novel technique that involves laser-assisted micromachining of silicon has recently been used to fabricate corrugated feedhorns that operate at terahertz frequencies [34]. These feedhorns will be used with SIS mixers and may eventually be used with photomixers.

Once the technology for photomixer LO's on space-based platforms develops, other applications will be possible. For example, bench-top measurements of molecular gases will be possible using the photomixer as a tunable source with unprecedented spectral brightness. The photomixer can also have a significant impact on millimeter and submillimeter-wave systems that require an oscillator with a very wide tuning bandwidth (0.2–100 GHz, or 0.1–4 THz) and with millisecond frequency agility.

ACKNOWLEDGMENT

The authors thank K. M. Molvar, W. F. DiNatale, K. B. Nichols, M. J. Manfra, and S. Calawa for assistance in sample growth and fabrication.

REFERENCES

[1] A. S. Pine, R. D. Suenram, E. R. Brown, and K. A. McIntosh, "A terahertz photomixing spectrometer: Application to SO_2 self broadening," *J. Mol. Spectrosco.*, vol. 175, pp. 37–47, 1996.

[2] D. E. Prober, "Superconducting terahertz mixer using a transition-edge microbolometer," *Appl. Phys. Lett.*, vol. 62, pp. 2119–2121, 1993.

[3] A. Skalare, W. R. McGrath, B. Bumble, H. G. LeDuc, P. J. Burke, A. A. Verheijen, R. J. Schoelkofp, and D. E. Prober, "Large bandwidth and low noise in a diffusion-cooled hot-electron bolometer mixer," *Appl. Phys. Lett.*, vol. 68, pp. 1558–1560, 1996.

[4] G. N. Gol'tsman, B. S. Karasik, O. V. Okunev, A. L. Dzardanov, E. M. Gershenzon, H. Ekstroem, S. Jacobsson, and E. Kollberg, "NbN hot electron superconducting mixers for 100 GHz operation," *IEEE Trans. Appl. Superconduct.*, vol. 5, pp. 3065–3068, June 1995.

[5] E. Gerecht, C. F. Musante, C. R. Lutz, Z. Wang, J. Bergendahl, K. S. Yngvesson, E. R. Mueller, J. Waldman, G. N. Gol'tsman, B. M. Voronov, and E. M. Gershenzon, "Hot electron mixing in NbN at 119-micrometer wavelength," in *Proc. Int. Semicond. Res. Symp.*, Univ. of Virginia, Charlottesville, Dec. 1995, pp. 619–622.

[6] K. A. McIntosh, E. R. Brown, K. B. Nichols, O. B. McMahon, W. F. DiNatale, and T. M. Lyszczarz, "Terahertz photomixing with diode lasers in low-temperature-grown GaAs," *Appl. Phys. Lett.*, vol. 67, pp. 3844–3846, 1995.

[7] E. R. Brown, K. A. McIntosh, K. B. Nichols, and C. L. Dennis, "Photomixing up to 3.8 THz in low-temperature-grown GaAs," *Appl. Phys. Lett.*, vol. 66, pp. 285–287, 1995.

[8] M. Hyodo, M. Tani, S. Matsuura, N. Onodera, and K. Sakai, "Generation of millimeter-wave radiation using a dual-longitudonal-mode microchip laser," *Electron. Lett.*, vol. 32, pp. 1589–1591, 1996.

[9] E. R. Brown, K. A. McIntosh, F. W. Smith, K. B. Nichols, M. J. Manfra, C. L. Dennis, and J. P. Mattia, "Milliwatt output levels and superquadratic bias dependence in a low-temperature-grown GaAs photomixer," *Appl. Phys. Lett.*, vol. 64, pp. 3311–3313, 1994.

[10] R. H. Kingston, *Detection of Optical and Infrared Radiation.* Berlin, Germany: Springer-Verlag, 1978.

[11] E. R. Brown, F. W. Smith, and K. A. McIntosh, "Coherent millimeter-wave generation by heterodyne conversion in low-temperature-grown GaAs photoconductors," *J. Appl. Phys.*, vol. 73, pp. 1480–1484, 1993.

[12] K. A. McIntosh, K. B. Nichols, S. Verghese, and E. R. Brown, "Investigation of ultrashort photocarrier relaxation times in low-temperature-grown GaAs," *Appl. Phys. Lett.*, vol. 70, pp. 354–356, 1997.

[13] N. F. Mott and R. W. Gurney, *Electronic Processes in Ionic Crystals.* London, U.K.: Oxford Univ. Press, 1940.

[14] U. Siegner, R. Fluck, G. Zhang, and U. Keller, "Ultrafast high-intensity nonlinear absorption dynamics in low-temperature-grown gallium arsenide," *Appl. Phys. Lett.*, vol. 69, pp. 2566–2568, 1996.

[15] J. P. Ibbetson and U. K. Mishra, "Space–charge-limited currents in nonstoichiometric GaAs," *Appl. Phys. Lett.*, vol. 68, pp. 3781–3783, 1996.

[16] M. A. Frerking, "Submillimeter source needs for NASA missions," *Proc. SPIE*, vol. 2145, pp. 222–227, 1994.

[17] E. R. Brown, J. R. Söderström, C. D. Parker, L. J. Mahoney, K. M. Molvar, and T. C. McGill, "Oscillations up to 712 GHz in InAs/AlSb resonant-tunneling diodes," *Appl. Phys. Lett.*, vol. 58, pp. 2291–2293, 1991; R. Blundell, D. C. Papa, E. R. Brown, and C. D. Parker, "Resonant-tunneling-diode oscillator as an alternative LO for SIS receiver applications," *Appl. Phys. Lett.*, vol. 29, pp. 288–289, 1993.

[18] J. S. Major, Jr., S. O'Brien, V. Vulgazov, D. F. Welch, and R. J. Lang, "High-power single-mode AlGaAs distributed Bragg reflector lasers diodes operating at 856 nm," *Electron. Lett.*, vol. 30, pp. 496–497, 1994.

[19] S. B. Waltman, L. W. Hollberg, K. A. McIntosh, E. R. Brown, "Demonstration of a phase-lockable microwave to submillimeter-wave sweeper," *SPIE*, vol. 2842, pp. 55–58, 1996.

[20] P. Chen, G. A. Blake, E. R. Brown, K. A. McIntosh, S. Y. Chou, M. I. Nathan, "Spectroscopic applications and frequency control of submillimeter-wave photomixing with distributed-Bragg-reflector diode lasers in low-temperature-grown GaAs," submitted for publication.

[21] S. B. Waltman, private communication, Jan. 1997.

[22] H. M. Pickett, private communication, Oct. 1996.

[23] P. L. Richards, "Bolometers for infrared and millimeter waves," *J. Appl. Phys.*, vol. 76, pp. 1–24, 1994.

[24] D. B. Rutledge, D. P. Neikirk, and D. P. Kasilingam, "Integrated circuit antennas," in *Infrared and Millimeter Waves*, K. J. Button, Ed. New York: Academic, 1983, vol. 10, pp. 1–90.

[25] P. R. Smith, D. H. Auston, and M. C. Nuss, "Subpicosecond photoconducting dipole antennas," *IEEE J. Quantum Electron.*, vol. 24, pp. 255–260, Feb. 1988.

[26] G. M. Rebeiz, "Millimeter-wave and terahertz integrated circuit antennas," *Proc. IEEE*, vol. 80, pp. 1748–1770, Nov. 1992.

[27] K. A. McIntosh, E. R. Brown, K. B. Nichols, O. B. McMahon, W. F. DiNatale, and T. M. Lyszczarz, "Terahertz measurements of resonant planar antennas coupled to low-temperature-grown GaAs photomixers," *Appl. Phys. Lett.*, vol. 69, pp. 3632–3634, 1996.

[28] J. S. Blakemore, "Semiconducting and other major properties of gallium arsenide," *J. Appl. Phys.*, vol. 53, pp. R123–R181, 1982.

[29] H. H. Wang, J. F. Whitaker, A. Chin, J. Mazurowski, and J. M. Ballingall, "Subpicosecond carrier response of unannealed low-temperature-grown GaAs vs temperature," *J. Electron. Mater.*, vol. 22, pp. 1461–1464, 1993.

[30] S. Calawa and A. R. Calawa, private communication, Oct. 1996.

[31] Y.-C. E. Tong and R. Blundell, private communicatoin, Oct. 1996.

[32] M. Gaidis and W. R. McGrath, private communication, Dec. 1996.

[33] P. F. Goldsmith, "Quasioptical techniques at millimeter and submillimeter wavelengths," in *Infrared and Millimeter Waves.* New York: Academic, 1982, vol. 6, pp. 277–342.

[34] C. K. Walker, T. M. Bloomstein, S. T. Palmacci, M. B. Stern, J. E. Curtin, "Laser micromachining of silicon: a new technique for fabricating high quality terahertz waveguide components," in *Proc. 8th Int. Symp. Space Terahertz Tech.*, Cambridge, MA, Mar. 25–27, 1997.

S. Verghese was born in Raleigh, NC, in 1965. He received the B.S. degree in physics and the B.S. and M.S. degrees in electrical engineering from North Carolina State University at Raleigh, in 1987, and the M.A. and Ph.D. degrees in physics from the University of California, Berkeley, in 1993.

In 1993, he was a Post-Doctoral Associate in the Department of Electrical Engineering and Computer Science, Massachusetts Institute of Technology (MIT), Cambridge, MA. In 1995, he joined the technical staff of the High-Speed Electronics Group at Lincoln Laboratory, MIT. His current research interests include submillimeter-wave sources, quantum-effect devices, and infrared detectors.

K. A. McIntosh received the B.S. degree in physics from the University of California at Davis in 1986.

Since joining Lincoln Laboratory, Massachusetts Institute of Technology (MIT), Cambridge, MA, in 1986, he has investigated high-speed optical and electronic devices. Some of his research has involved the application of intersubband transitions in quantum wells for novel infrared devices. His current interests include the ultrafast optoelectronic properties of low-temperature-grown III–V materials and devices, as well as the development of new photonic crystal materials.

E. R. Brown (M'92) received the M.S. and Ph.D. degrees in applied physics from the California Institute of Technology, Pasadena, CA, in 1981 and 1985, respectively.

In 1985, he joined the research staff of Lincoln Laboratory, Massachusetts Institute of Technology (MIT), Cambridge, MA, where he worked in the area of millimeter-wave and infrared quantum electronics. His research focused on resonant-tunneling devices, quantum-well intersubband devices including IR detectors and modulators, THz coherent sources (photomixers) made from low-temperature-grown GaAs, novel heterostructure transistors, microwave applications of photonic-crystal structures, and novel methods in environmental sensing. From 1992 to 1996, he was a Project Leader and Assistant Group Leader in the High-Speed Electronics Group at Lincoln Laboratory. Since 1996, he has been a Program Manager with DARPA/ETO, Arlington, VA, where he manages programs in revolutionary microwave and mm-wave technology, infrared artifical dielectrics, megawatt sold-state switching technology, and sonoelectronics (advanced acoustic imaging technology).

Dr. Brown is a member of the American Physical Society, the AAAS, and the New York Academy of Sciences.